Hindawi
Shock and Vibration
Volume 2022, Article ID 8232065, 20 pages
https://doi.org/10.1155/2022/8232065

Research Article

Seismic Signal-Based Investigation on the Disaster Differences between 2021 Yangbi Ms 6.4 Earthquake and 2014 Ms 6.5 Ludian Earthquake in Yunnan Province, China

Jinchang Chen,[1] Ailan Che ,[1] Lanmin Wang,[1,2] and Lixin Jiang[3]

[1]*School of Naval Architecture, Ocean and Civil Engineering, Shanghai Jiao Tong University, Shanghai 200040, China*
[2]*Lanzhou Institute of Seismology, China Earthquake Administration, Lanzhou 730000, China*
[3]*China Earthquake Networks Center, Beijing 100045, China*

Correspondence should be addressed to Ailan Che; alche@sjtu.edu.cn

Received 11 April 2022; Revised 25 June 2022; Accepted 7 July 2022; Published 1 August 2022

Academic Editor: Annalisa Greco

An Ms 6.4 earthquake occurred in Yangbi County, Yunnan Province, on May 21, 2021. The magnitude is only 0.1 difference when compared with the 2014 Ms 6.5 earthquake in Ludian County, Yunnan Province, but the disasters show a big difference. Seismic signal includes the comprehensive information of source, propagation path, and site effect, which directly reflect the effect of the earthquake on the ground. The study mainly investigated the difference between seismic signals of two events in time domain and time-frequency-energy space based on variational mode decomposition and Hilbert transform to clarify the reasons for disaster differences. Most damaged buildings are column-and-tie timber structures with Earth walls with local collapse or vertical crack at the corner of the Earth wall in the Yangbi earthquake. Multistorey buildings are intact, and a few small landslides are triggered, whereas, in the Ludian earthquake, multistorey buildings with the frame structure and masonry structure occurred with serious X-type cracking, large interlayer displacement, and even complete collapse, and large landslides with length about 165 m are triggered. 53LLT and 53YBX are two strong motion stations in the Ludian earthquake and Yangbi earthquake, respectively, and are near the disaster investigation points. Peak ground acceleration in 53LLT is up to 949.2 cm/s^2, which is larger than 720.3 cm/s^2 in 53YBX, and the duration in 53LLT is longer than 53YBX. The instantaneous energy of 53YBX is concentrated within 0–10 Hz and 10–20 Hz, respectively; however, the instantaneous energy of 53LLT is concentrated at 5 Hz. Cumulative energy of 53YBX is mainly distributed at 0–5 Hz and 10–20 Hz, which is around the natural frequency of column-and-tie timber structure, while the energy of 53LLT is concentrated at 1.6 Hz and is much greater than other stations. Thus, large energy in high frequency caused the instantaneous and cumulative damage to short-period structures in Yangbi County and may cause the resonance of column-and-tie timber structure, and large energy in low frequency caused the instantaneous and cumulative damage to long-period structures of Longtou Village in Ludian earthquake. The result is meaningful to understanding the seismic disasters from the characteristics of seismic signals and can provide a reference for the seismic design of structures.

1. Introduction

Yunnan Province is located on the eastern edge of the collision zone between the Indian Plate and the Eurasian Plate and the southern section of the North-South Seismic Belt of China. There are 49 active faults developed in the Yunnan Province [1], with strong tectonic movement and significant seismic activity. It is one of the areas with earthquakes most active in the world [2, 3]. By 2021, 189 earthquakes of Ms 4.6 or higher than Ms 4.6 had occurred in the area, including 49 earthquakes of Ms 4.6–5.0, 107 earthquakes of Ms 5.0-6.0, and 33 earthquakes of Ms 6.0–7.8. According to the earthquake records since the 20th century, earthquakes with M 5.0~5.9 in Yunnan occur twice a year, earthquakes with M 6.0~6.9 occur twice every three years, and earthquakes with M 7 and above occur about once every eight years [4]. Large casualties and losses are caused by the frequent occurrence of earthquakes. Particularly in 2014, there were 8 destructive earthquakes with $M \geq 5.0$ in Yunnan (including 5 with M 5.0~5.9 and 3 with M 6.0~6.9), and the

economic losses, deaths, disappearances, and injuries accounted for 84.03%, 99.2%, 100%, and 97.86%, respectively, in the same period at China [5], in which most of casualties and losses are induced by the Ms 6.5 Ludian earthquake. On May 21, 2021, another destructive earthquake with a magnitude Ms 6.4 occurred in Yangbi County, Yunnan Province. The disasters present a big difference when compared with the Ludian earthquake.

Seismic signal is a vibration phenomenon that occurs when energy is suddenly released and propagated to the ground after long-term accumulation, which is the comprehensive reflection of source, propagation path, and site effect [6]. It is the starting point and essential basis of scientific research on seismology and earthquake engineering. At present, we mainly investigate the seismic signal through amplitude, duration, and spectrum. The peak ground acceleration (PGA) and the peak ground velocity (PGV) are usually used as a sign of earthquake intensity [7]. Two factors were also widely used in the structural seismic vulnerability analysis [8, 9]. However, PGA value cannot reflect the earthquake damage degree reasonably. For example, in the 1985 Mexico earthquake, the recorded PGA was only 0.17 g, which was much smaller than 0.6 g recorded in the 1986 San Salvador earthquake, but caused more serious earthquake damage [10]. Reference [11] pointed out that PGA represents the amplitude of the high-frequency component of seismic signal and has great discreteness. The experimental and case investigation show that the types of structural damage mainly include instantaneous damage and cumulative damage, and many motions with small amplitude but long duration are very destructive to the structure [12]. Therefore, seismic duration has a great impact on the cumulative damage of structures. Amplitude and duration of seismic signals are the characteristics of the time domain. Under the effect of earthquakes, the dynamic response of the structure is closely related to the spectrum characteristics of seismic signal. When the dominant frequency band is close to the natural frequency of the structure, the structural response will be significantly amplified, resulting in serious damage to the structure [13]. If the frequency of the seismic signal is concentrated in the high-frequency band, the short-period structure will cause great harm, and when the predominant frequency of the seismic signal is in the low-frequency band, it will lead to great damage to the long-period structure. In the Peru earthquake on October 17, 1966, the seismic damage in Lima City was mainly concentrated in single-storey houses, and there was little damage to multistorey houses. According to the seismic signal records of Lima City, the predominant period is nearby 0.1 s, and the natural vibration period of single-storey houses is just close to 0.1 s.

Fourier transform is widely used in the dynamic response of the structure under seismic ground motion [14, 15]. However, previous study works show that the Fourier transform is only applicable to linear and stationary data analysis [16, 17]. Compared with the Fourier transform, the Hilbert-Huang transform (HHT) can be used for nonlinear and nonstationary signal and has been widely used in analyzing seismic signals in recent years [17–20]. However, empirical mode decomposition (EMD) of HHT essentially belongs to recursive modal decomposition. The envelope estimation error is amplified by multiple recursive decomposition, which is prone to modal aliasing, and the decomposition result is greatly affected by the sampling rate [21]. Aiming at the problems of EMD, [22] proposed variational mode decomposition (VMD), which is a nonrecursive, self-adaptive, and multiresolution signal decomposition method. VMD overcomes the problems of mode aliasing and error accumulation of EMD [23, 24]. VMD combined with Hilbert transform (HT) was used in the study.

We investigated the disasters of the epicenter of the 2021 Yangbi Ms 6.4 earthquake and the 2014 Ms 6.5 Ludian earthquake at first. The disasters show a big difference, even the magnitude with only 0.1 difference. Then, we analyzed the characteristics of seismic signals in the two events from the time domain and time-frequency-energy space which is based on VMD and HT. The result of the study can help us know better about the relationship between seismic disasters and the seismic signals and provide a reference for the seismic design of structures.

2. Cases Study

2.1. Earthquake Events. An Ms 6.4 earthquake occurred in Yangbi County, Dali City, Yunnan Province (Figure 1), on May 21, 2021, with a focal depth of 8 km. It was another destructive earthquake with a magnitude greater than 6 in Yunnan Province after the Ludian Ms 6.5 earthquake, Jinggu Ms 6.6 earthquake, and Yingjiang Ms 6.1 earthquake in 2014. The seismogenic structure of the earthquake is a secondary fault on the west side of the Weixi-Qiaohou fault, which is dominated by dextral strike-slip movement [25]. Before Ms 6.4 earthquake, four earthquakes with a magnitude of Ms 4.2, Ms 5.6, Ms 4.5, and Ms 2.8 occurred successively on the same day. By June 15, 2021, there were more than 40 aftershocks with a magnitude beyond Ms 3.0 in Yangbi County, including 2 earthquakes above Ms 5.0. The largest aftershock was the Ms 5.2 earthquake (25.59°N, 99.97°E) on May 21, 2021 (43 minutes after the mainshock) [26]. Therefore, the earthquake sequence is a typical foreshock-mainshock-aftershock sequence. The earthquake caused 3 deaths, 32 injuries, 13000 damaged buildings and triggered a few small landslides. The epicenter intensity is up to VIII (China seismic intensity scale). According to the intensity map made by the Yunnan Province earthquake administration (Figure 1), the area of the VI region is about 5500 km^2, the area of the VII region is 930 km^2, and the area of the VIII region is 170 km^2. A total of 46 landslides, 6 collapses, and 7 debris flows were triggered in the earthquake. All of them have small or medium volume and are mainly distributed in the VIII and VII regions [27].

Compared with other earthquakes (Ms > 6) that occurred in Yunnan Province, especially for Ludian Ms 6.5 earthquake, the building damage degree, landslides number, casualties, and economic loss caused by the Yangbi earthquake were much less. Ludian earthquake (Figure 1) occurred on August 3, 2014; the epicenter intensity was up to IX, and the focal depth was about 12 km, which caused 617 deaths, 2400 injuries, 86000 destroyed buildings and

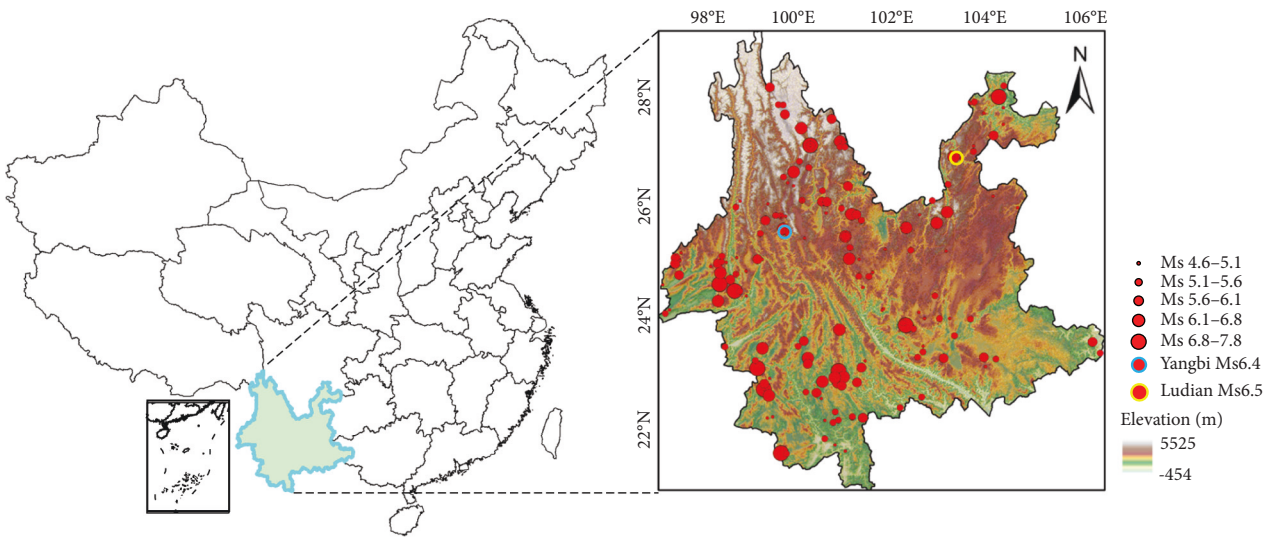

Figure 1: The location of the 2021 Yangbi and 2014 Ludian earthquakes.

triggered many large landslides [28, 29]. According to the survey data of the Department of Natural Resources of Yunnan Province, China, 986 landslides and 462 collapses were triggered. Most of them are large and huge landslides. Among them, the Hongshiyan landslide and Ganjiazhai landslide are two largest landslides with a total volume of more than 10 million m^3. Fifty-five people were buried in the Ganjiazhai landslide.

2.2. Topographic Characteristics. The elevation and slope angle shown in Figures 2 and 3 present the topography characteristics of the area within the intensity map of the Yangbi earthquake and Ludian earthquake, respectively. The elevation within the intensity map of two earthquakes changes from 1070 m to 4180 m and from 434 m to 4003 m, respectively. Figure 4(a) shows that elevation within 1500 m–2500 m in different intensity regions of two earthquakes takes the largest ratio. It takes 72.8%, 67.6%, and 99.3% in the VI region, VII region, and VIII region, respectively, for the Yangbi earthquake and takes 61.6%, 70.0%, 74.7%, and 78.9% in the VI region, VII region, VIII region, and IX region, respectively, for Ludian earthquake. The slope angle within the intensity map of two earthquakes changes from 0° to 71.98° and from 0° to 85.99°, respectively. The slope angle (Figure 4(b)) within 10–20° takes the largest ratio. Areas with a slope angle larger than 30° take 11.5%, 17.9%, and 10.6% in the VI region, VII region, and VIII region, respectively, for the Yangbi earthquake and takes 23.7%, 19.8%, 27.2%, and 30.4% in the VI region, VII region, VIII region, and IX region, respectively, for Ludian earthquake. It shows that the elevation distribution characteristics in different intensity regions of two earthquakes are close, but the slope angle larger than 30° in different intensity regions of the Ludian earthquake takes a higher ratio than that of the Yangbi earthquake.

2.3. Characteristics of Disasters. After the Yangbi Ms 6.4 earthquake, we investigated the damage degree of buildings and geotechnical disasters at Xiajie Village (in Yangbi County), Huaian Village, and Shahe Village, which are within or close to the epicenter and the 53YBX strong motion station, as it is shown in Figure 2(a). Typical seismic damage phenomenon in the Yangbi earthquake is shown in Figure 5. The structural types of buildings in the areas mainly include adobe and timber, brick and timber, and brick and concrete. Based on the investigation, we found that adobe and timber building takes the largest ratio among the damaged buildings. The damage of this structural type mainly occurred at the Earth wall, as it is shown in Figure 5. At Xiajie Village (Figure 5(a)), the Earth wall of adobe and timber structure mainly made local collapse at corner, while the brick and concrete with multistorey at Xiajie Village is stable, as it is shown in the last two pictures of Figure 5(a). At Huaian and Shahe Village (Figures 5(b)–5(c)), the Earth wall of adobe and timber structure mainly made vertical cracks at corner. At Shahe Village, a few small landslides are triggered (Figure 5(d)), which block the road.

The damaged adobe and timber buildings in the Yangbi earthquake belong to traditional Chinese column-and-tie timber structures, as shown in Figure 6. The upper load and weight of the whole roof are transmitted from rafters to purlins, then from purlins to column, and through column to the ground. Chuanfang plays an important role in connecting wooden columns and enhancing the stability of the whole frame and has little contribution to load bearing. The column is the main load-bearing member. The construction sequence of the building is as follows: the wooden column is built at first, and then the Chuanfang is used to connect the columns to establish the timber frame. On this basis, the Earth wall is built. Finally, purlin is installed, and rafters and ties are erected to complete the main construction of the building. The seismic behavior of it is poor because of lacking effective earthquake resistance measures. Its natural frequency is around 10 Hz [30].

Compared with the Yangbi earthquake, the damage phenomenon induced by the Ludian earthquake presents different characteristics. Figure 7 shows the typical seismic

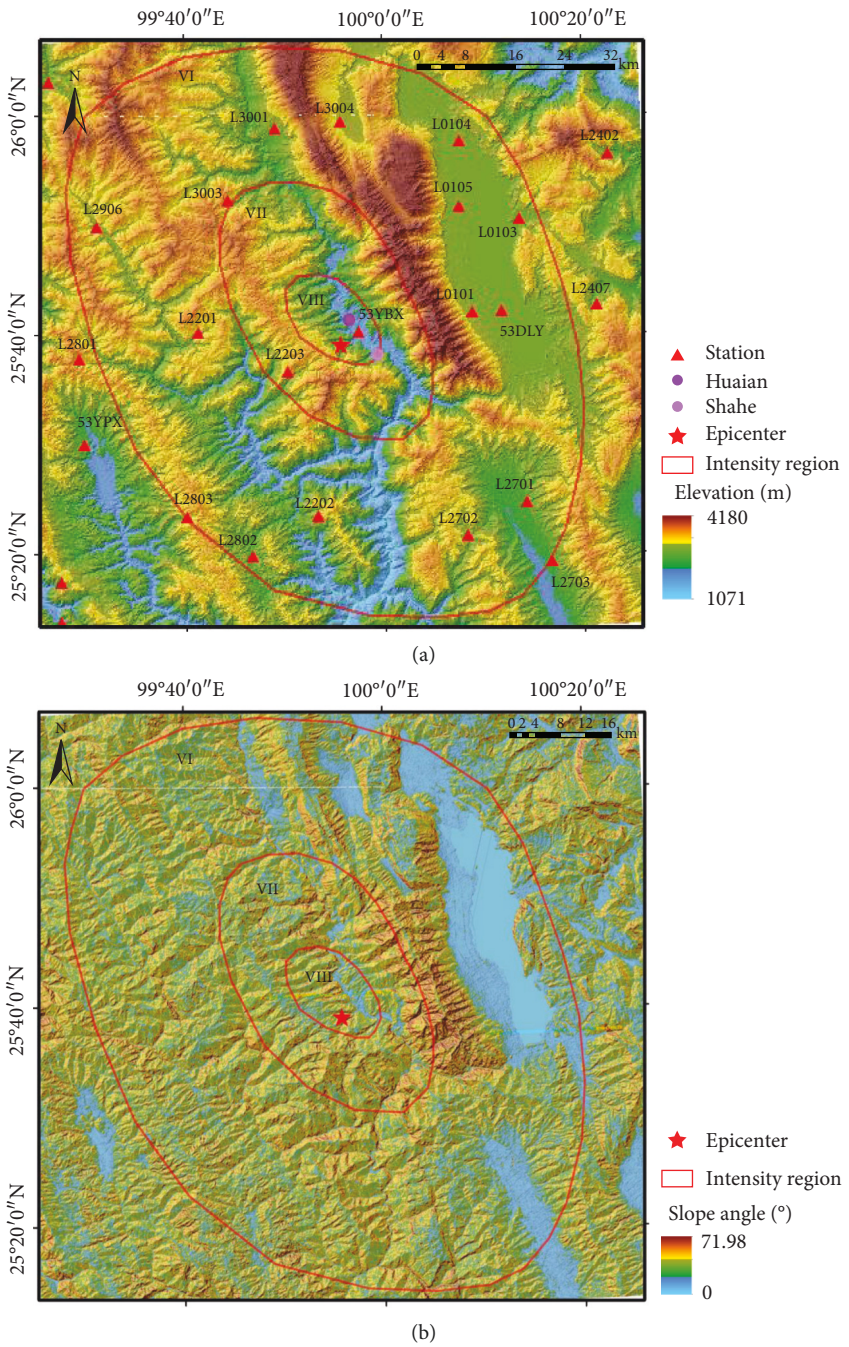

Figure 2: Distribution of elevation, slope angle, and intensity map in Yangbi earthquake. (a) Elevation and intensity map. (b) Slope angle and intensity map.

damage phenomenon in Longtou Village, which is near the 53LLT strong motion station, as it is shown in Figure 3(a). The structural types of buildings in Longtou Village mainly include frame structure, masonry structure, timber structure, and adobe and timber. In Longtou Village, frame structure and masonry structure with multistorey are seriously damaged. Figure 7(a) shows that serious X-type cracking and large interlayer displacement occurred at these buildings, and many of them even collapsed completely. Large landslides with a length of about 165 m also occurred at Longtou Village, as shown in Figure 7(b), which destroyed and buried part of the buildings. It shows that seismic damage caused by the Ludian earthquake is much more serious than the Yangbi earthquake, although the two events all occurred in Yunnan Province, and the magnitude is only 0.1 difference.

3. Data and Method

3.1. Strong Motion Data. In the Yangbi earthquake, 17 strong motion stations distributed within the intensity map record this event, including 1 in the VIII region, 1 in the VII

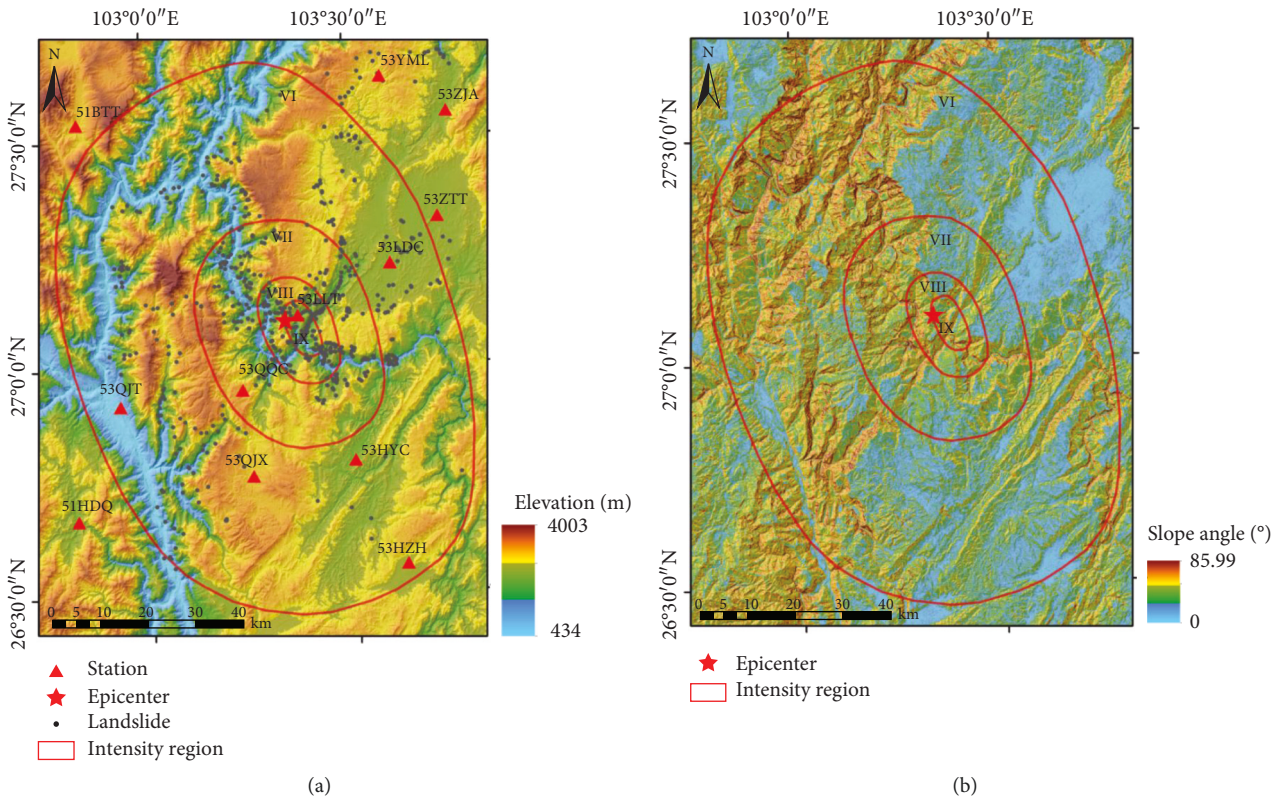

Figure 3: Distribution of elevation, slope angle, and intensity map in Ludian earthquake. (a) Elevation and intensity map. (b) Slope angle and intensity map.

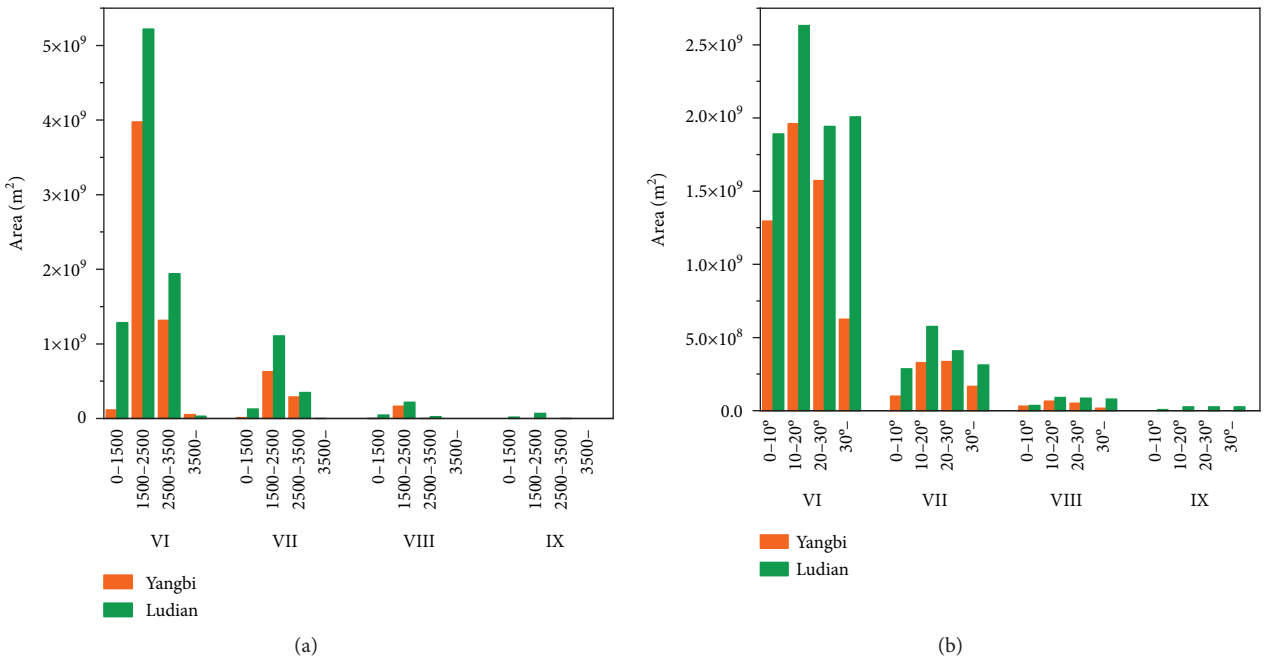

Figure 4: Distribution areas of elevation and slope angle in different intensity regions of two events. (a) Elevation. (b) Slope angle.

(a)

(b)

(c)

(d)

Figure 5: Typical seismic damage phenomenon in Yangbi Ms 6.4 earthquake. (a) Damaged buildings in Xiajie Village, Yangbi County. (b) Damaged buildings in Huaian Village. (c) Damaged buildings in Shahe Village. (d) Small landslides in Shahe Village.

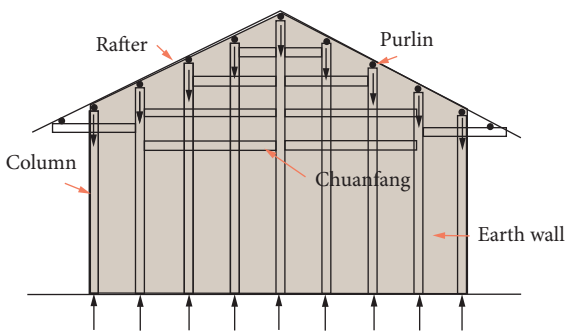

Figure 6: Column-and-tie timber structure with Earth wall.

region, and 15 in the VI region. In the Ludian earthquake, 7 strong motion stations distribute in the intensity map, including 1 in the IX region, 1 in the VII region, and 5 in the VI region. Table 1 shows the basic information of the strong motions with the epicentral distance within 40 km of two earthquakes. The 53YBX and 53LLT with an epicentral distance of around 8 km are near the disaster investigation points of two earthquakes, which give a valuable opportunity to study the disaster differences according to the characteristics of seismic signals. The baseline correction and Butterworth filter with 0.1–30 Hz bandwidth were applied to these strong motion recordings.

3.2. Method

3.2.1. Variational Mode Decomposition (VMD). The Intrinsic Mode Function (IMF) is defined as an amplitude-modulated-frequency-modulated signal, as shown in

$$u_k(t) = A_k(t)\cos(\phi_k(t)), \tag{1}$$

(a)

(b)

Figure 7: Typical seismic damage phenomenon in Longtou Village in Ludain Ms 6.5 earthquake. (a) Damaged buildings. (b) Landslides.

Table 1: Basic information of strong motion stations in the study.

Events	Station	Site condition	Epicentral distance (km)	Intensity scale	PGA (cm/s^2)		
					EW	NS	UD
Yangbi earthquake	53YBX	Soil	8.6	VIII	379.8	720.3	448.4
	L2203	Soil	10	VII	196.2	310.0	188.0
	L2201	Soil	16.6	VI	64.7	70.0	49.6
	L3003	Rock	25.6	VI	81.4	71.7	39.3
	L2202	Soil	30.5	VI	80.7	72.4	54.3
Ludian earthquake	53LLT	Soil	8.3	IX	949.2	−705.8	−504.4
	53QQC	Soil	18.7	VII	−146.0	−140.3	−52.8
	53LDC	Soil	32.5	VI	−45.9	44.8	−25.6
	53QJX	Soil	38	VI	135.2	−133.4	65.0
	53HYC	Rock	39.6	VI	88.3	87.7	47.5

where $\phi_k'(t) \geq 0$, $A_k(t) \geq 0$, instantaneous frequency $\omega_k(t) = \phi_k'(t)$ varies much slower than $\phi_k(t)$, and k is the number of IMFs. On the interval $[t-\delta, t+\delta]$, $\delta \approx 2\pi/\phi_k'(t)$, the mode $u_k(t)$ is a pure harmonic signal.

VMD is a process of solving the variational problem, which can minimize the sum of the estimated bandwidth of each mode. In order to estimate the bandwidth of modes, firstly, the unilateral spectrum is obtained by the Hilbert transform. Then, the modal spectrum is modulated to the fundamental frequency band by mixing the central frequency. Finally, the demodulated signal is processed by Gaussian smoothing. The constrained variational problem for estimating the bandwidth of modes is shown in the following equation:

$$\min_{\{u_k\},\{\omega_k\}} \left\{ \sum_k \left\| \partial_t \left[\left(\delta(t) + \frac{j}{\pi t} \right) * u_k(t) \right] e^{-j\omega_k t} \right\|_2^2 \right\}, \quad \sum_k u_k = f, \tag{2}$$

where $\{u_k\} = \{u_1, u_2, \ldots, u_k\}$ are the IMFs, $\{\omega_k\} = \{\omega_1, \omega_2, \ldots, \omega_k\}$ are the central frequency of each IMF, and $\delta(t)$ is the pulse function.

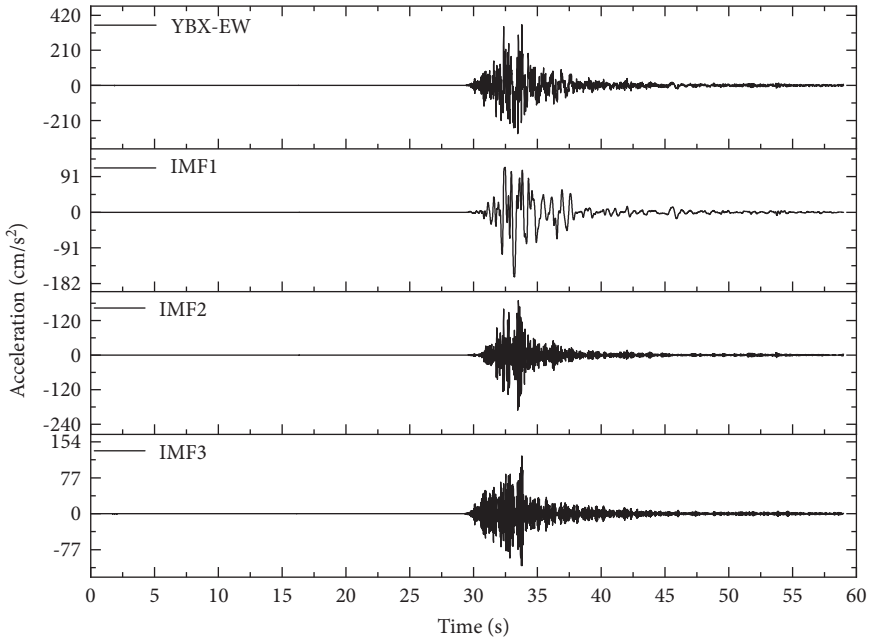

Figure 8: VMD result of the seismic signal (53YBX-EW).

The quadratic penalty term (α) and Lagrange multipliers ($\lambda(t)$) are introduced to solve the problem. The augmented Lagrangian function is as follows:

$$\mathscr{L}(\{u_k\},\{\omega_k\},\lambda) := \alpha\sum_k \left\|\partial_t\left[\left(\delta(t)+\frac{j}{\pi t}\right)*u_k(t)\right]e^{-j\omega_k t}\right\|_2^2 + \left\|f(t)-\sum_k u_k(t)\right\|_2^2 + \langle\lambda(t), f(t)-\sum_k u_k(t)\rangle. \tag{3}$$

In order to solve equation (3), Alternating Direction Method of Multipliers (ADMM) is used by iteratively updating u_k, ω_k, and λ. The specific steps are as follows: (1) $\{u_k^1\}$, $\{\omega_k^1\}$, λ^1, and n are initialized to 0; (2) $\hat{u}_k$, ω_k, and λ are iteratively updated by equations (4)–(6), respectively; (3) repeat steps (2) to (3) until the iteration termination conditions (equation (7)) are met:

$$\hat{u}_k^{n+1}(\omega) = \frac{\hat{f}(\omega)-\sum_{i\neq k}\hat{u}_i(\omega)+\hat{\lambda}(\omega)/2}{1+2\alpha(\omega-\omega_k)^2}, \tag{4}$$

$$\omega_k^{n+1} = \frac{\int_0^\infty \omega|\hat{u}_k(\omega)|^2 d\omega}{\int_0^\infty |\hat{u}_k(\omega)|^2 d\omega}, \tag{5}$$

$$\hat{\lambda}^{n+1}(\omega) = \hat{\lambda}^n(\omega)+\tau\left(\hat{f}(\omega)-\sum_k \hat{u}_k^{n+1}(\omega)\right), \tag{6}$$

$$\sum_k \frac{\|\hat{u}_k^{n+1}-\hat{u}_k^n\|_2^2}{\|\hat{u}_k^n\|_2^2} < \varepsilon, \tag{7}$$

where ε is the accuracy, $\varepsilon > 0$.

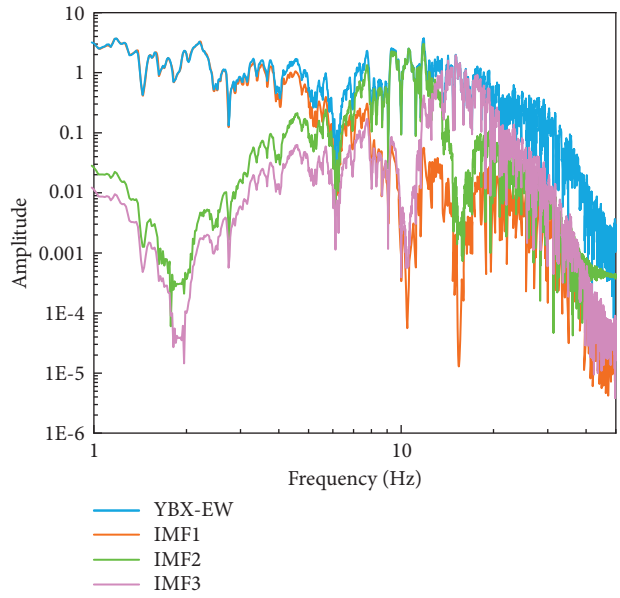

Figure 9: Fourier spectrums of the 53YBX-EW and its IMFs.

The number of IMFs is set to 3 in the study. It is taken according to the number of predominant frequencies of the Fourier spectrum. Figures 8 and 9 are the VMD result of 53YBX-EW and its Fourier spectrum, respectively. The Fourier spectrum of the original signal and its three IMFs indicates that the three predominant frequencies are around 2 Hz, 10 Hz, and 15 Hz, respectively.

3.2.2. Hilbert Transform (HT). IMF is acquired by VMD, and each of them is well behaved in the Hilbert transform. The Hilbert transform $y(t)$ is shown in the following equation [17]:

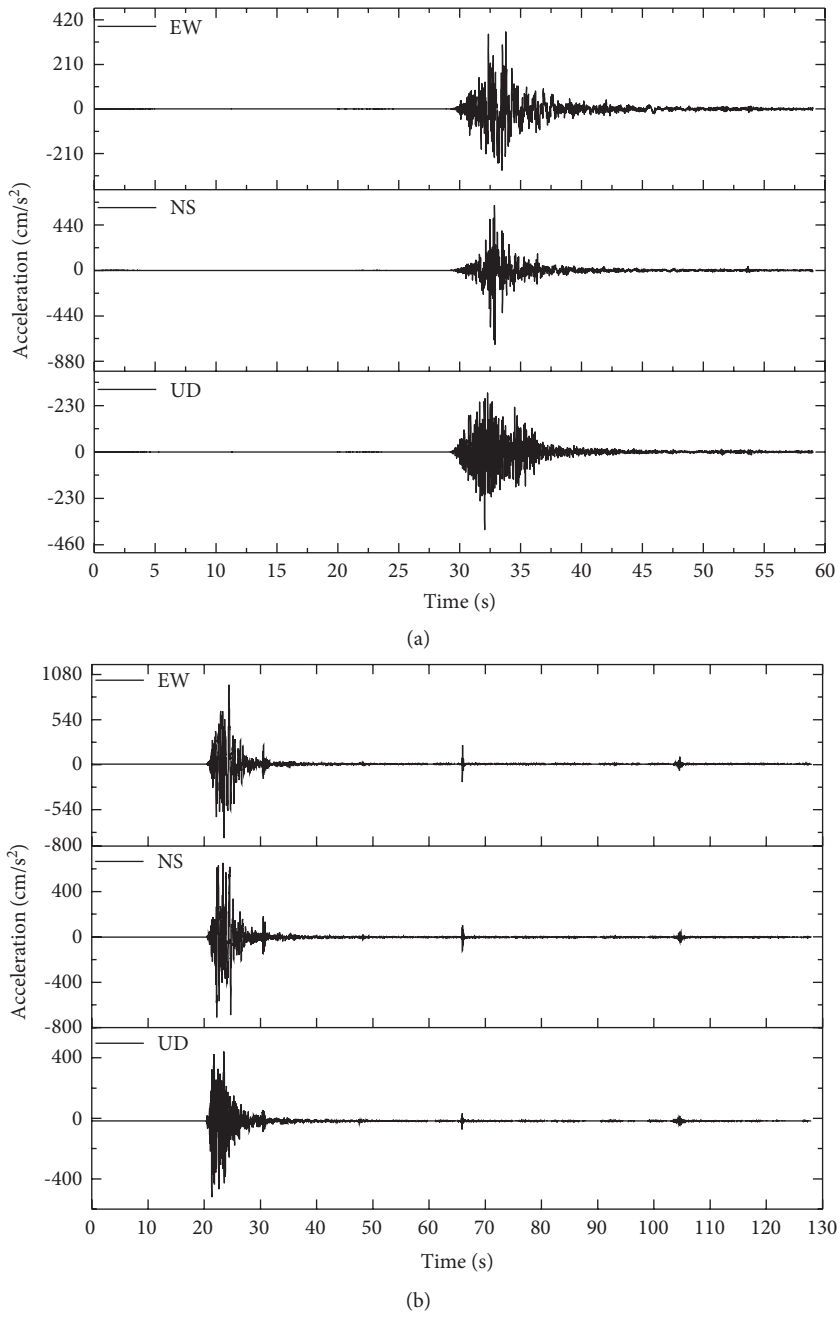

Figure 10: Acceleration time history of (a) 53YBX and (b) 53LLT.

$$y(t) = H[x(t)] = \frac{1}{\pi} P\left(\int_{-\infty}^{\infty} \frac{x(\tau)}{t-\tau} d\tau \right), \tag{8}$$

where $x(t)$ is the time history of the signal, which is equal to $u(t)$ in this study, and P is the Cauchy principal value.

An analytic signal $z(t)$ can be defined as

$$z(t) = x(t) + jy(t) = a(t)e^{j\theta(t)}. \tag{9}$$

The calculation method of $a(t)$ and $\theta(t)$ is shown in equations (10) and (11), respectively:

$$a(t) = \sqrt{x^2(t) + y^2(t)}, \tag{10}$$

$$\theta(t) = \arctan \frac{y(t)}{x(t)}. \tag{11}$$

The instantaneous frequency ($\omega(t)$) is the first derivative of $\theta(t)$ to time equation.

$$\omega(t) = \frac{d\theta(t)}{\mathrm{dt}}. \tag{12}$$

The Hilbert spectrum $H(t, \omega)$ is shown in the following equation:

$$H(t,w) = \sum_{1}^{m} a_i(t,w_i). \quad (13)$$

The marginal spectrum $h(w)$ is the integral of $H(t, \omega)$ over time, as shown in the following equation:

$$h(w) = \int_0^T H(t,w)\mathrm{d}t. \quad (14)$$

4. Characteristics of Seismic Signals

4.1. Time Domain Characteristics. Major characteristics such as PGA and duration of seismic wave record by the strong motion station can be acquired in the time domain.

The acceleration time history of 53YBX and 53LLT is shown in Figure 10. 53YBX station is 8.6 km away from the epicenter, and the PGAs in three directions were 379.8 cm/s^2 (EW), 720.3 cm/s^2 (NS), and 448.4 cm/s^2 (UD), respectively. 53LLT station is 8.3 km away from the epicenter, and the PGAs in three directions were 949.2 cm/s^2 (EW), −705.8 cm/s^2 (NS), and −504.4 cm/s^2 (UD), respectively. PGA attenuation rules of the two events are shown in Figure 11. In soil site, with the increase of epicentral distance, PGA in three directions has a decreasing tendency. In rock sites, PGA has a certain degree of increase. We should pay attention to the fact that PGA increases obviously at QJX, which may relate to the local landform.

The duration of an earthquake can reflect the cumulative damage effect of seismic signals on structures. There are two kinds of seismic signal duration, which are absolute duration and relative duration. In the earthquake engineering field, we mainly study the relative duration, which focuses on the strong part of seismic signals. Kawashima bracketed duration, which is a kind of relative duration, was used in the study to investigate the duration characteristics. It takes the duration of the first and last times reaching or exceeding 1/5~1/2 of the maximum peak acceleration as the duration, also known as fractional duration or relative peak duration. In this study, 0.3 is selected for calculation and analysis. The duration of strong motions of two earthquakes is shown in Table 2. The distribution of the duration is relatively discrete. In the Yangbi earthquake, the minimum duration is 2.1 s (53YBX-NS), and the maximum duration is 13.4 s (L3003-UD). In the Ludian earthquake, the minimum duration is 4.3 s (53LLT-UD), and the maximum duration is 15.3 s (53LDC-NS). The maximum PGA of two earthquakes occurred at 53YBX-NS and 53LLT-EW, respectively, and the duration of 53YBX-NS is less than 53LLT-EW, which indicates that the seismic signal of 53LLT has much cumulative damage effect on structures.

4.2. Time-Frequency-Energy Space Characteristics. Based on VMD and HT, the time-frequency-energy distribution characteristics of seismic waves can be obtained, which are mainly presented in the Hilbert spectrum and marginal spectrum in the study. The Hilbert spectrum reflects the distribution of time, frequency, and instantaneous energy. The marginal spectrum is the integral of the Hilbert spectrum over time, which can clarify the cumulative energy of every instantaneous frequency in the whole duration.

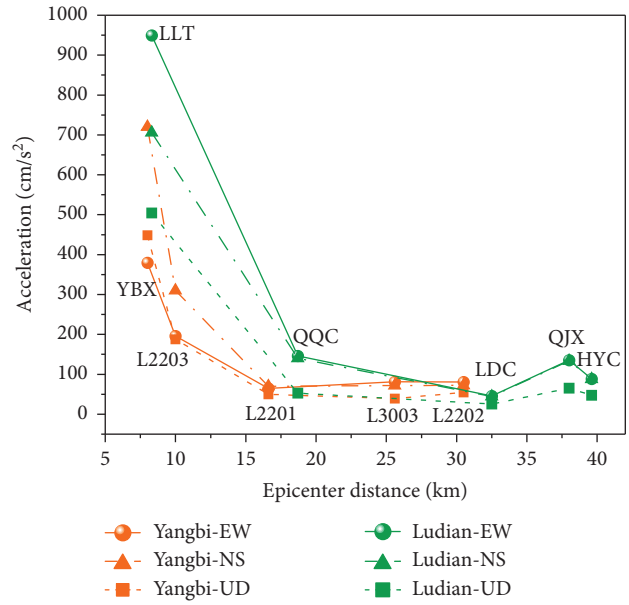

Figure 11: Attenuation of the PGA.

Table 2: Duration of strong motions.

Events	Station	Duration (s)		
		EW	NS	UD
Yangbi earthquake	53YBX	4.9	2.1	5.1
	L2203	4.6	2.3	5.9
	L2201	9.6	11.5	11.1
	L3003	12.2	11.7	13.4
	L2202	5.5	7.2	6.8
Ludian earthquake	53LLT	5.0	4.9	4.3
	53QQC	11.4	12.1	14.4
	53LDC	11.5	15.3	15.2
	53QJX	13.3	10.1	13.4
	53HYC	12.1	12.1	9.0

4.2.1. Hilbert Spectrum. The acceleration time history recorded by strong motion station has three components, and each of them contains meaningful information on seismic signals. In the time domain, it is not easy to synthesize the three components for the amplitude depending on the direction. Most studies mainly investigated the single component and ignored the others. However, in time-frequency-energy space, three components all present the distribution of time, frequency, and energy which are scalar. The synthesized Hilbert spectrum can reflect the instantaneous energy distribution of the seismic wave of a strong motion station completely. The Hilbert spectrums of 53YBX in three directions are shown in Figure 12. In the EW direction (Figure 12(a)), the energy is mainly distributed at 0–10 Hz and 10–20 Hz, respectively. However, in NS and UD directions (Figures 12(b)-12(c)), energy is mainly distributed at 10–20 Hz. The synthesized Hilbert spectrum of

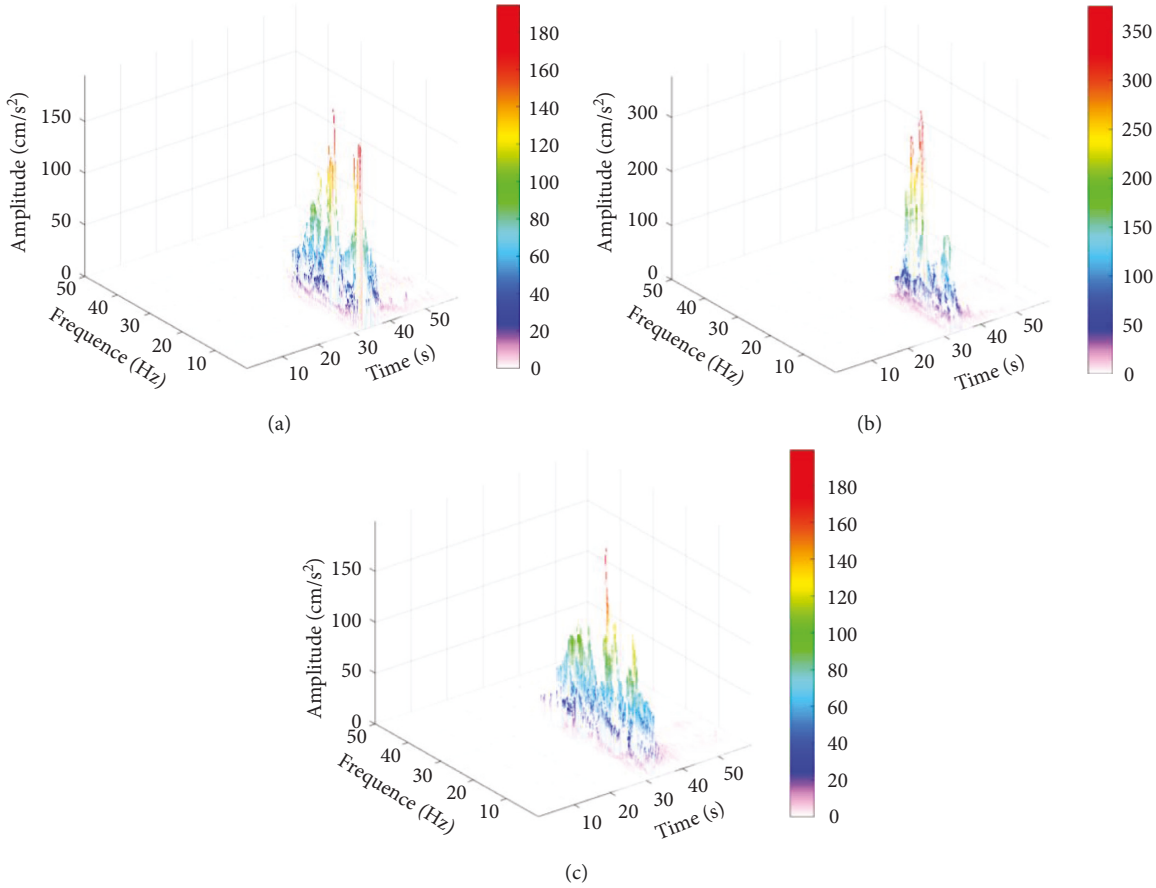

Figure 12: Hilbert spectrums of 53YBX in three directions. (a) 53YBX-EW. (b) 53YBX-NS. (c) 53YBX-UD.

53YBX is shown in Figure 13(a); two predominant frequencies are clearly clarified.

Hilbert spectrums of seismic waves recorded by different stations in the Yangbi earthquake are shown in Figures 13(a)–13(e). The shape of 53YBX presents double-peak, which are within 0–10 Hz and 10–20 Hz, respectively. However, the shape of others presents a single peak, and the instantaneous energy is mainly concentrated within 20 Hz. With the increase of epicentral distance, the energy shows a downward trend. However, the peak instantaneous energy has a slight increase in L3003 (from 52 cm/s^2 in L2201 to 73 cm/s^2 in L3003), which indicates that the soil layer can absorb peak instantaneous energy. Hilbert spectrums of seismic waves recorded by different stations in the Ludian earthquake are shown in Figures 13(f)–13(j). The shape of them shows a single peak, and the energy is mainly concentrated within 20 Hz. The peak instantaneous energy of them occurred within 10 Hz. The energy also shows a downward trend with the increases of epicentral distance, and the peak energy at the rock site (53HYC) is greater than that at the soil site when the epicentral distance is close. It should be noted that the energy at 53QJX has a significant increase in 53QJX (from 50 cm/s^2 in LDC to 130 cm/s^2 in 53QJX), which may be caused by its special site conditions and need to be investigated furtherly in our later works. The energy of 53LLT is concentrated at 5 Hz and the peak up to 1280 cm/s^2, which has a significant destructive instantaneous effect on long-period buildings. Compared with 53LLT, 53YBX contains relatively large energy in high-frequency (>10 Hz) parts, which has a destructive instantaneous effect on the short-period structures.

4.2.2. Marginal Spectrum. Marginal spectrums of seismic waves in the Yangbi earthquake are shown in Figure 14(a). In 53YBX, cumulative energy is mainly distributed in two frequency ranges, which are 0–5 Hz and 10–20 Hz, respectively. In other stations, cumulative energy is mainly distributed within 10 Hz. Peak cumulative energy shows a decreasing trend with the increases of epicentral distance, which is independent of site conditions. Marginal spectrums in the Ludian earthquake are shown in Figure 14(b). In 53LLT, the predominant frequency is 1.6 Hz, and the corresponding amplitude is much greater than it in other stations. The predominant frequency of other stations is within 3.8 Hz–4.3 Hz. Peak cumulative energy also shows a decreasing trend with the increases of epicentral distance. However, at 53QJX, cumulative energy shows an abnormal increase. This phenomenon also shows the Hilbert spectrum. Comparing the marginal spectrum of 53YBX with 53LLT, the difference is obvious. For 53LLT, large cumulative energy is concentrated at low frequency, which can induce the cumulative damage of long-period structures. For 53YBX, a large part of cumulative energy

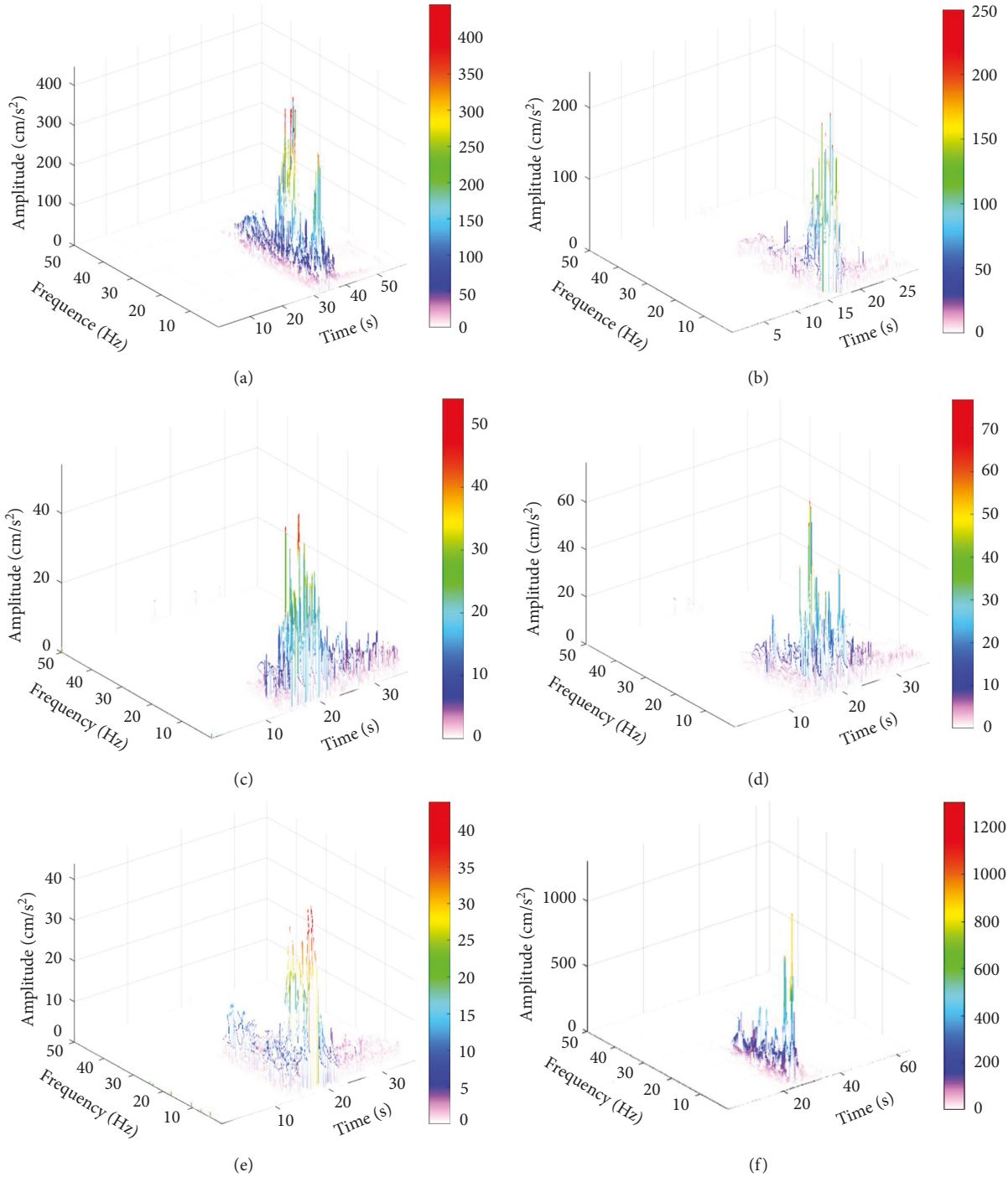

Figure 13: Continued.

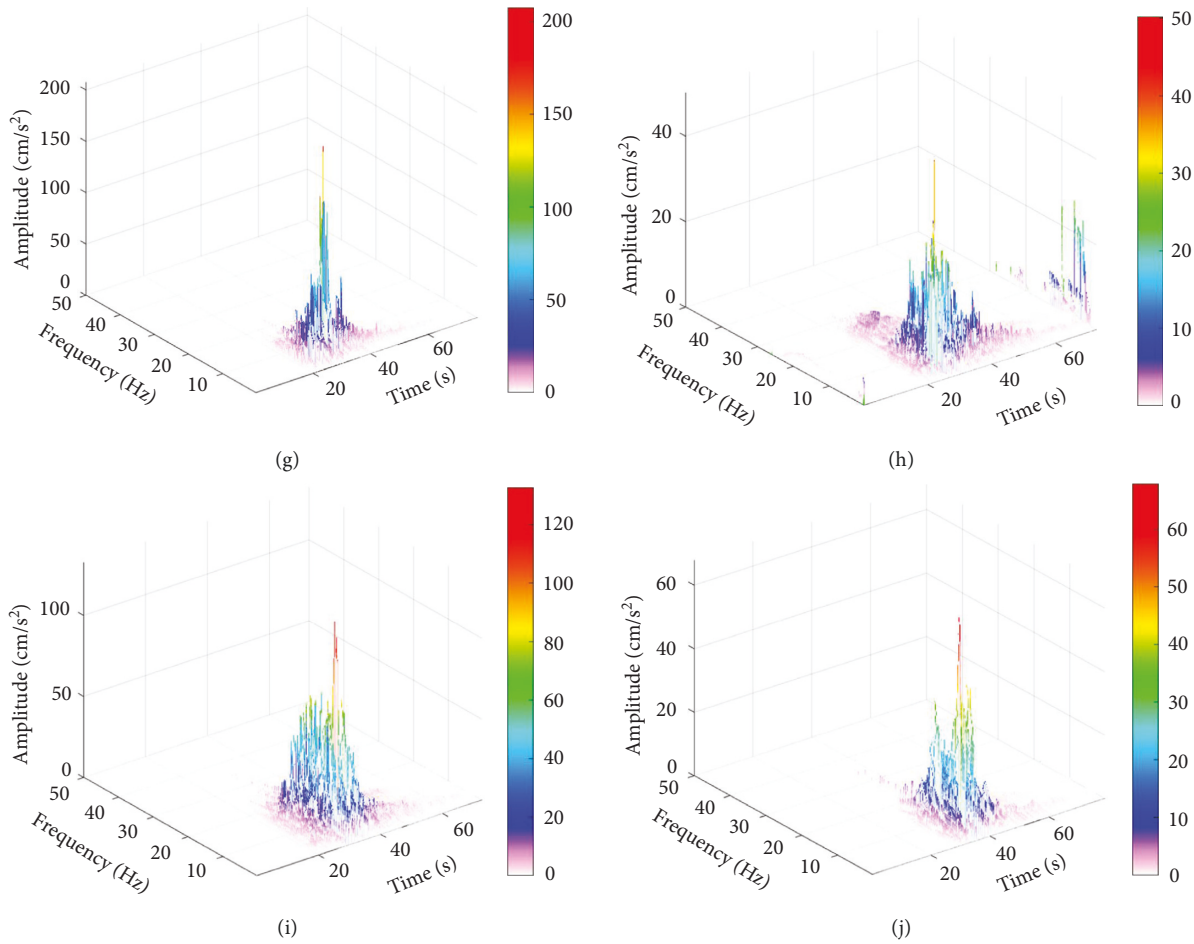

Figure 13: Hilbert spectrums of seismic wave in Yangbi earthquake and Ludian earthquake. (a) 53YBX. (b) L2203. (c) L2201. (d) L3003. (e) L2202. (f) 53LLT. (g) 53QQC. (h) 53LDC. (i) 53QJX. (j) 53HYC.

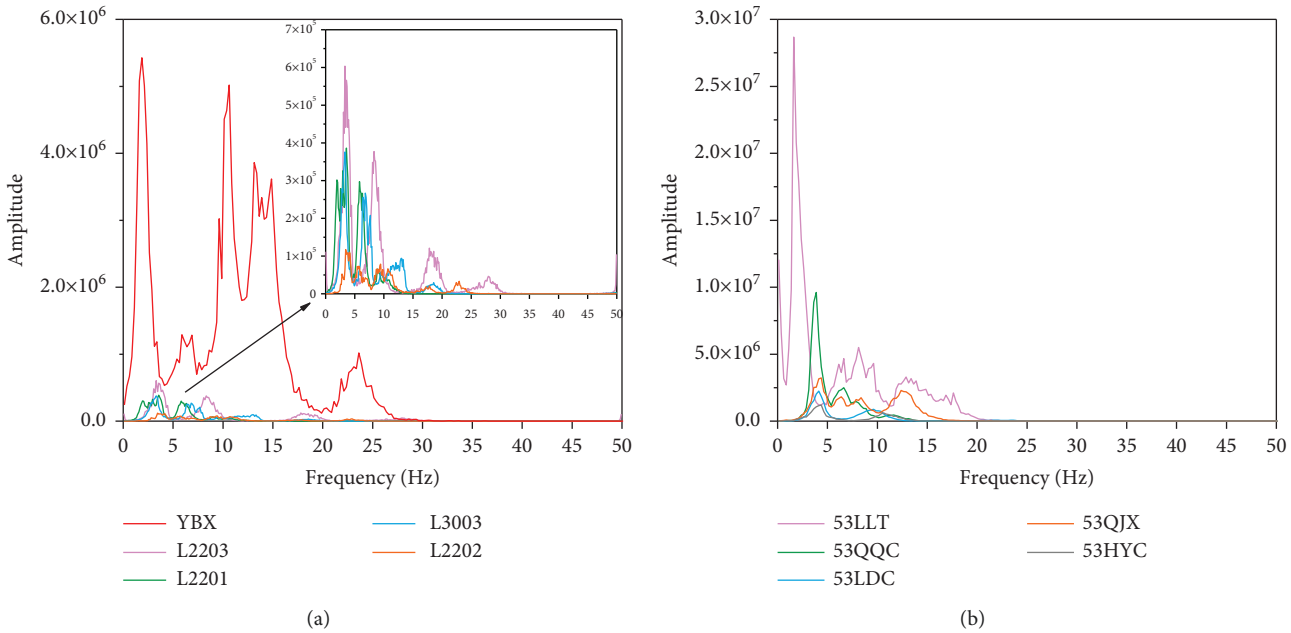

Figure 14: Marginal spectrums of seismic wave in Yangbi earthquake and Ludian earthquake. (a) Yangbi earthquake. (b) Ludian earthquake.

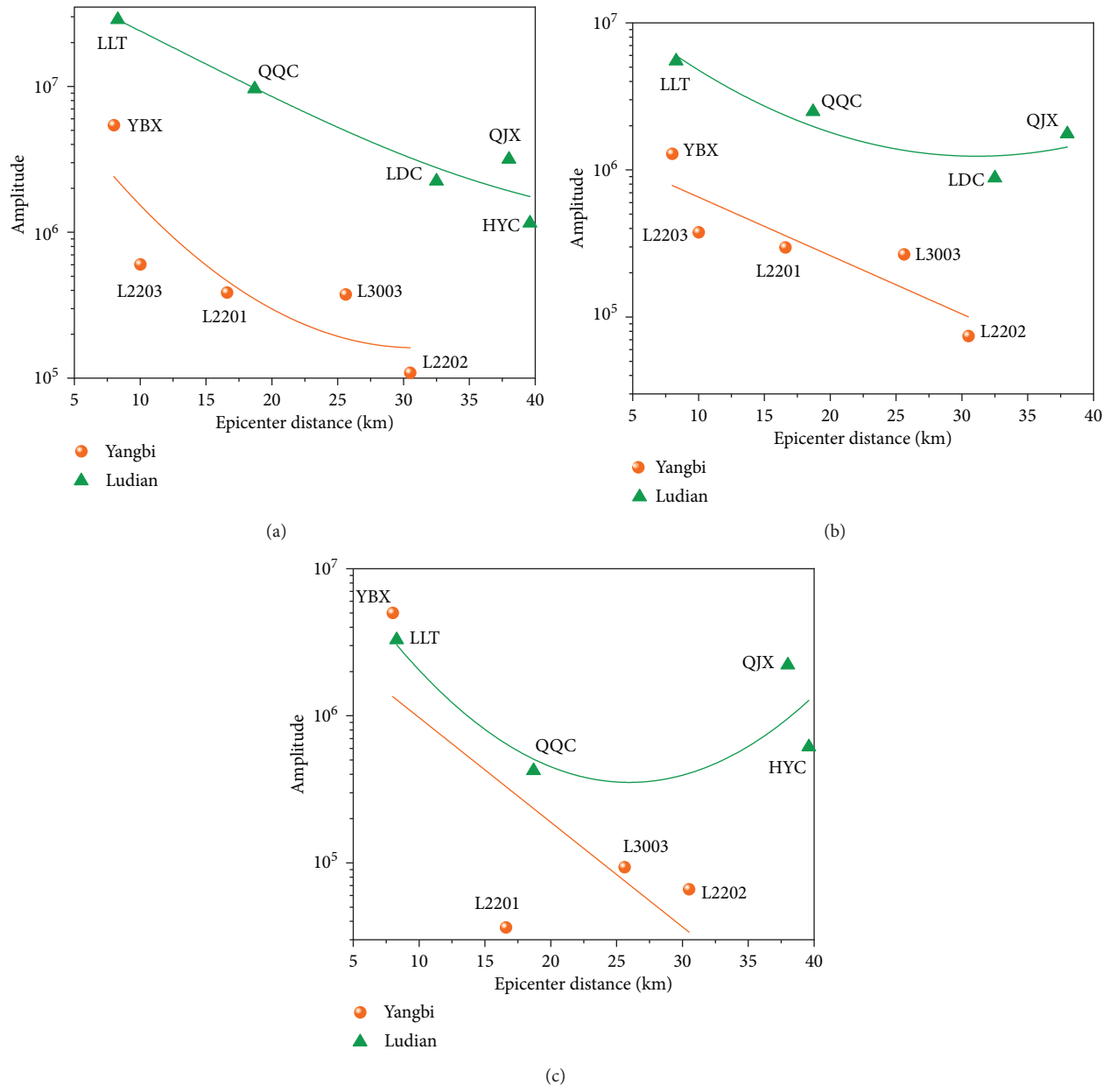

Figure 15: Attenuation of cumulative energy within different frequency ranges of the two events. (a) 0–5 Hz. (b) 5–10 Hz. (c) 10–15 Hz.

is concentrated at a high frequency, which can cause cumulative damage to the short-period structures.

According to the distribution characteristics of cumulative energy shown in Figure 14, we mainly investigate the attenuation rules of cumulative energy in three frequency ranges which are 0–5 Hz, 5–10 Hz, and 10–15 Hz, as it is shown in Figure 15. In three frequency ranges, with the increase of epicentral distance, the cumulative energy of the Yangbi earthquake decays faster than the energy of the Ludian earthquake. The energy of the Ludian earthquake is greater than the Yangbi earthquake when the epicentral distance is close. The result reflects that the seismic wave of the Ludian earthquake contains larger cumulative energy than the Yangbi earthquake and attenuates more slowly, which can cause more serious damage. It should be noticed that the energy in 10–15 Hz of 53YBX is even larger than 53LLT, although there is a 0.1 magnitude of difference between the two earthquakes, and the epicentral distance of the two stations is close. As mentioned above, the natural frequency of damaged buildings (column-and-tie timber structure with Earth wall) in the Yangbi earthquake is around 10 Hz. Large cumulative energy in high frequency (10–15 Hz) may cause the resonance of the structure. So, short-period structures in the Yangbi earthquake suffered serious cumulative damage.

5. Discussion

5.1. Effect of Frequency of Seismic Wave on Slope and Building. Disasters caused by two events show a big difference. In the Yangbi earthquake, the casualties and economic loss are

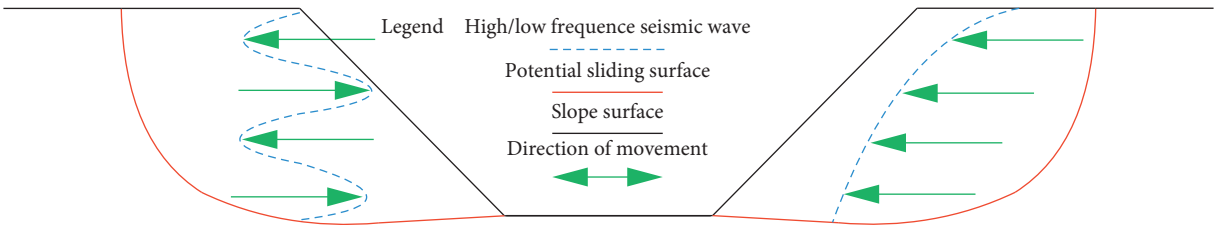

Figure 16: Effect of frequency of seismic wave on slope (modified from [31]).

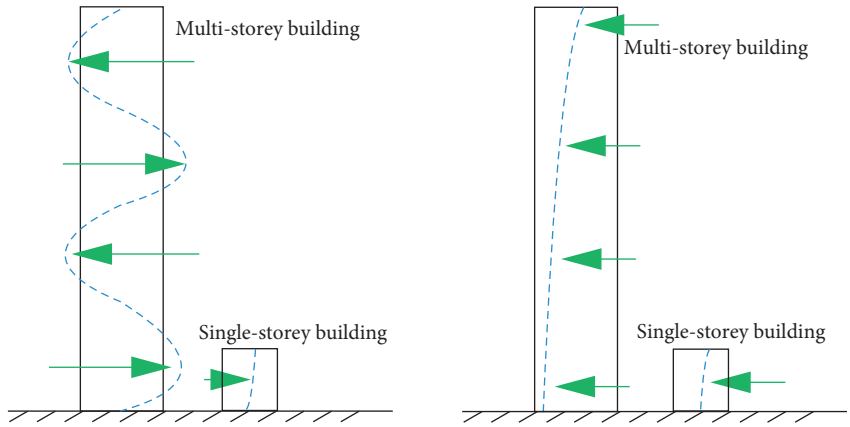

Figure 17: Effect of frequency of seismic wave on building.

minor. The most damaged building type is adobe and timber with single-storey and with local collapse or vertical crack occurring at the corner of retaining wall. There is no obvious damage to multistorey buildings. However, the epicenter of the Ludian earthquake suffered great damage. Frame structure and masonry structure with multistorey caused serious X-type cracking and large interlayer displacement and even complete collapse. Meanwhile, large landslides with a length of 165 m were triggered.

The effect of the frequency of a seismic wave on the movement of the slope is shown in Figure 16. In theory, a high-frequency seismic signal with a shorter wavelength than the dimensions of slopes is unlikely to trigger landslides because high-frequency seismic waves drive different parts of the slope in the opposite direction simultaneously, so the whole slope would remain stable. On the other hand, low-frequency seismic wave with a longer wavelength than dimensions of slopes can lead slope to move in the same direction, which is more likely to induce landslides [31]. Similarly, the frequency of seismic wave has the same effect on the building (Figure 17). The low-frequency seismic wave would lead multistorey building to move in the same direction, and the building easily collapsed. On the contrary, the building would remain stable under the effect of high frequency of the seismic wave. It is in accord with the damage phenomenon of slope and buildings in Yangbi County and Longtou Village. This study shows that 53LLT contains large instantaneous energy and cumulative energy in low-frequency parts; however, 53YBX contains large energy in high-frequency parts. Thus, the large energy in high frequency caused instantaneous and cumulative damage to short-period structures in Yangbi County. Accordingly, the large energy in low frequency caused instantaneous and cumulative damage to long-period structures (multistorey buildings) and large landslides in Longtou Village.

5.2. Site Effect Characteristics. In order to investigate the site effect in two events, we use the horizontal to vertical Fourier spectral ratio (HVSR) of seismic signals to evaluate it. The method is proposed by Nakamura [32–34] and has developed into a standard technique to study site effects [35, 36]. The expression is shown in equation (15). In the study, the Fourier spectrum of the horizontal seismic signal is the synthetic seismic signal of EW and NS. Similarly, we calculated the horizontal to vertical marginal spectral based on the VMD and Hilbert transform (VHT) ratio of seismic signals in order to compare with the ratio based on the fast Fourier transform (FFT).

HVSR results based on FFT and VHT, respectively, are shown in Figure 18. The change rules of the FFT ratio and VHT ratio of different stations in two earthquakes are close. Two methods can recognize the predominant frequency of the sites, and the predominant frequency value is close. However, the amplitude has a certain difference, and the predominant frequency recognized by the VHT ratio is clearer than that by the FFT ratio. Peak amplitude (with FFT ratio 26 and VHT ratio 49) occurred at 53QJX, and the predominant frequency is about 5 Hz, which indicates that relatively large instantaneous energy and cumulative energy here are related to the local site conditions. The amplification effects (amplitude) of 53YBX and 53LLT are not obvious compared with other stations, which reflects that the distribution of instantaneous energy and cumulative

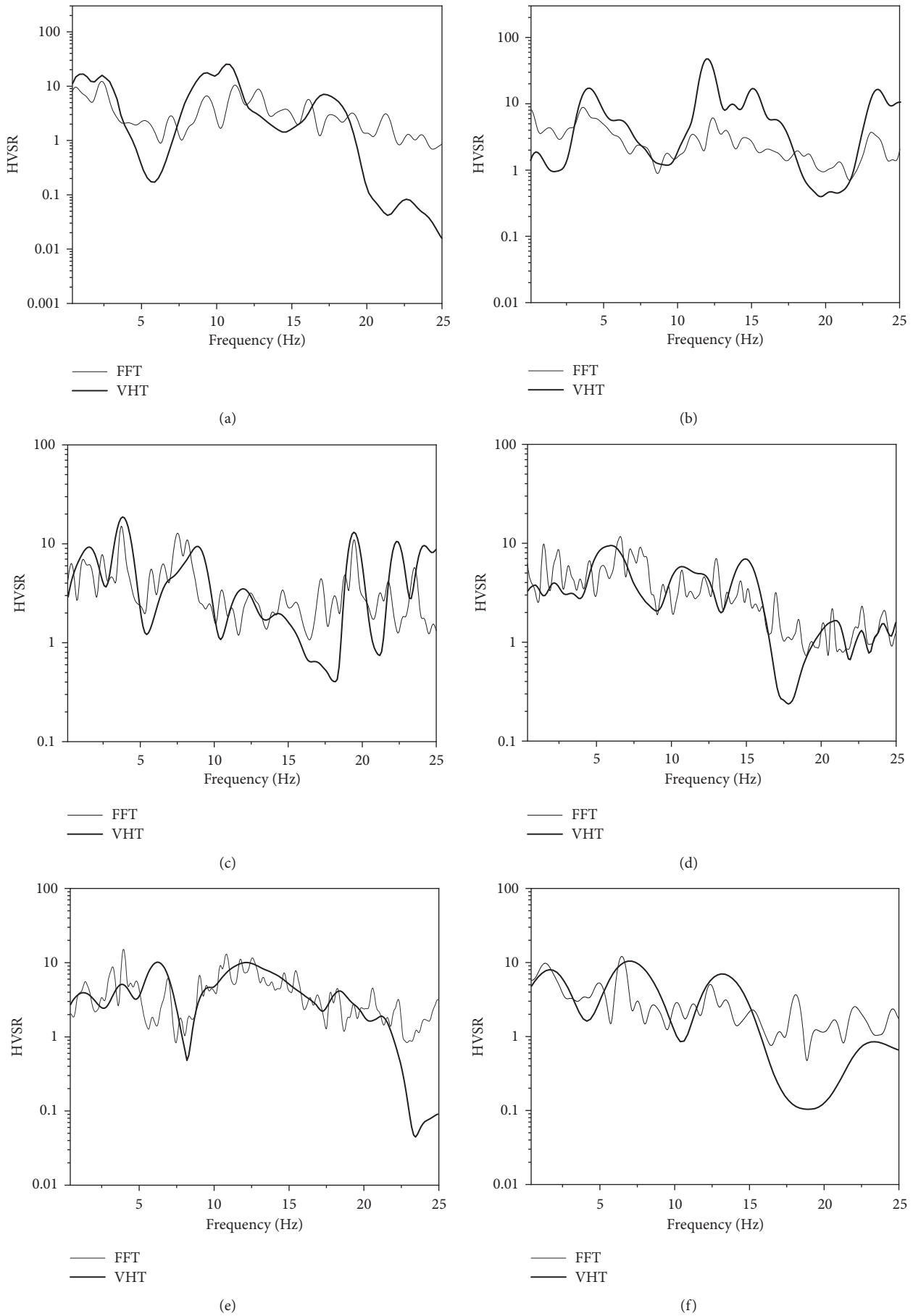

Figure 18: Continued.

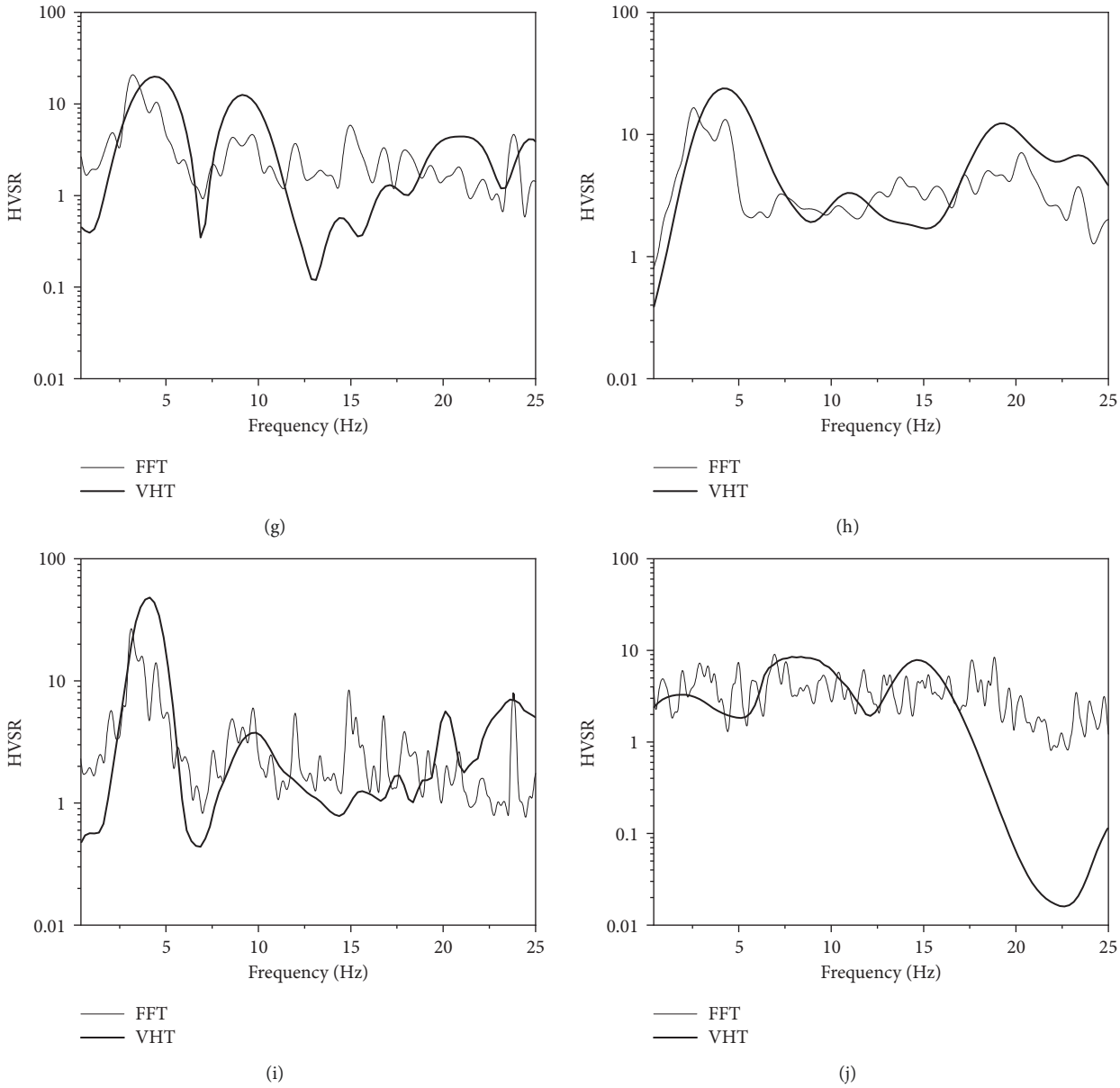

Figure 18: HVSRs based on FFT and VHT of the two events. (a) 53YBX. (b) L2203. (c) L2201. (d) L3003. (e) L2202. (f) 53LLT. (g) 53QQC. (h) 53LDC. (i) 53QJX. (j) 53HYC.

energy of the two stations mainly reflected the hypocenter characteristics.

$$R(f) = \frac{H(f)}{V(f)}, \tag{15}$$

where $H(f)$ is the Fourier spectrum of the horizontal seismic signal and $V(f)$ is the Fourier spectrum of the vertical seismic signal.

5.3. Low-Frequency Pulse Signal Extraction Based on VMD Method. Many studies have been done on the reasons for the large disaster in Longtou town caused by the Ludian earthquake. One main reason among them is the large-amplitude pulse contained in the time history of 53LLT [37–39]. Pulse-type seismic signal has more complex characteristics than ordinary seismic signal and can lead to serious damage to engineering structures [40, 41]. The Port Hueneme Mw 4.7 earthquake in 1957, the Parkfield Mw 5.6 earthquake in 1966, and the San Fernando Mw 6.6 earthquake in 1971 all showed the characteristics of small magnitude and serious disasters, and pulse-type seismic signals were recorded in these events [42, 43]. So, there is a need to identify, extract, and model the pulse-type seismic signal for further structural seismic analysis. However, the identification method requires visual inspection or repeat using wavelet transform [44, 45], and the method is based on the velocity time history of the seismic signal. In this study, an identification or extraction method using acceleration time history is proposed.

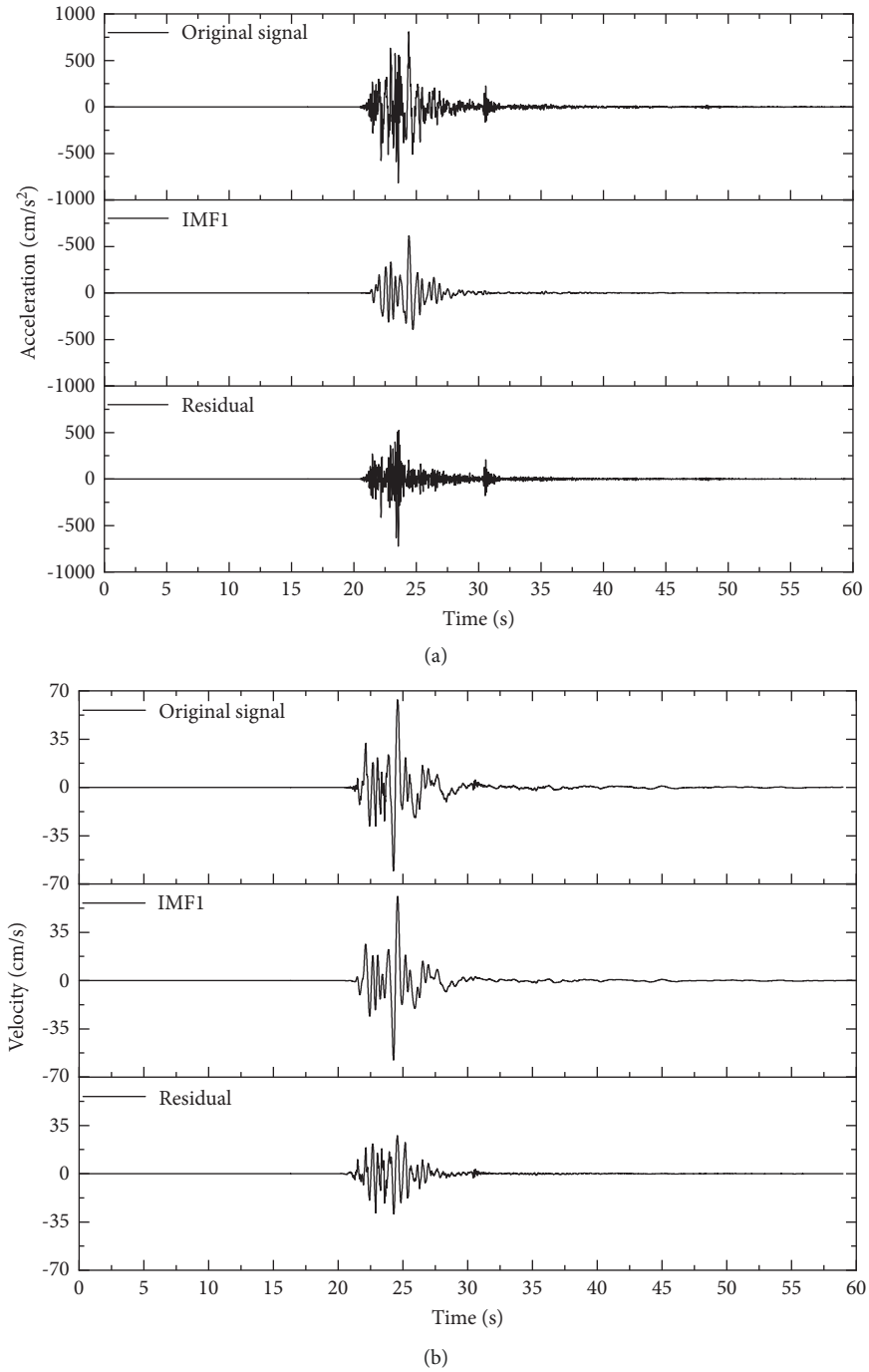

Figure 19: Acceleration and velocity time history of 53LLT (EW). (a) Acceleration time history. (b) Velocity time history.

Figure 19(b) shows the velocity time history of 53LLT (EW), which is the integral of the acceleration time history of 53LLT (EW) shown in Figure 19(a). The result shows that 53LLT (EW) contains a short-term velocity pulse of around 25 s, and IMF1 is the major component of the short-term velocity pulse of the original signal. The method based on VMD can effectively extract the pulse components from the acceleration time history of the seismic signals.

6. Conclusions

An Ms 6.4 earthquake occurred in Yangbi County, Yunnan Province, on May 21, 2021. Compared with Ms 6.5 Ludian earthquake that occurred in Yunnan Province on 2014, the disasters have a big difference, even the magnitude with 0.1 difference. The study mainly introduced the difference in seismic signals of epicenters of two earthquakes. The main conclusions are shown as follows.

The Yangbi Ms 6.4 earthquake caused 3 deaths, 32 injuries, 13000 damaged buildings and triggered a few small landslides. The epicenter intensity is VIII. Column-and-tie timber structure with Earth wall caused local collapse or vertical crack at the corner of Earth wall, which takes the largest ratio among the damaged buildings at the epicenter, and the multistorey buildings do not have obvious damage phenomenon. The Ludian Ms 6.5 earthquake caused 617 deaths, 2400 injuries, 86000 destroyed buildings and triggered many large landslides. The epicenter intensity is up to IX. Frame structure and masonry structure with multistorey in epicenter caused serious X-type cracking, large interlayer displacement, and even complete collapse.

PGAs of 53YBX in three directions are 379.8 cm/s^2 (EW), 720.3 cm/s^2 (NS), and 448.4 cm/s^2 (UD), and the PGAs of 53LLT in three directions are 949.2 cm/s^2 (EW), −705.8 cm/s^2 (NS), and −504.4 cm/s^2 (UD). PGA in the Ludian earthquake attenuates faster than that in the Yangbi earthquake with the increases of epicentral distance, and the duration in 53LLT is longer than 53YBX. The large PGA and long duration of the seismic signal may cause serious damage to the building in Longtou Village.

The Hilbert spectrum shape of 53YBX presents a double peak, and the instantaneous energy is concentrated within 0–10 Hz and 10–20 Hz, respectively. The Hilbert spectrum shape in the Ludian earthquake shows a single peak. The instantaneous energy of 53LLT is concentrated at 5 Hz, and the peak is up to 1280 cm/s^2, which may have a significant destructive instantaneous effect on long-period buildings. The marginal spectrum shows that, in 53YBX, cumulative energy is mainly distributed in two frequency ranges, which are 0–5 Hz and 10–20 Hz, respectively. In 53LLT, the predominant frequency is 1.6 Hz, and the cumulative energy is much greater than that in other stations. The large energy in low frequency caused instantaneous and cumulative damage to long-period structures in Longtou Village. The large energy in high frequency caused instantaneous and cumulative damage to short-period structures in Yangbi County and may cause the resonance of column-and-tie timber structure.

Data Availability

Basic data can be obtained from the corresponding author when needed. Data for this study are provided by the Institute of Engineering Mechanics, China Earthquake Administration.

Conflicts of Interest

The authors declare that they have no conflicts of interest.

Acknowledgments

This research work was supported by the National Key R&D Program of China (2018YFC1504506 and 2018YFC1504504) and the Key Project of National Natural Science Foundation of China (no. U1939209).

References

[1] X. W. An, Z. F. Chang, and Y. J. Chen, *Quaternary Active Faults in Yunnan*, Seismological Press, Beijing, China, 2018.

[2] W. C. Li, G. Deng, W. Cao, C. Xu, J. Chen, and M. L. Lee, "Discrete element modeling of the Hongshiyan landslide triggered by the 2014 Ms 6.5 Ludian earthquake in Yunnan, China," *Environmental Earth Sciences*, vol. 78, no. 16, p. 520, 2019.

[3] G. Huangfu, Y. Chen, and J. Z. Qin, *Seismicity in Yunnan, Kunming*, Yunnan Science and Technology Press, Kunming, China, 2010.

[4] S. G. He, H. Ran, Q. Y. Zhou, J. Yu, W. D. Luo, and X. F. Bai, "Seismic reinforcement performance of civil structure houses during Yangbi Ms 6.4 earthquake," *China Earthquake Engineering Journal*, vol. 43, no. 4, pp. 799–806, 2021, (In Chinese).

[5] Y. Q. Zhang, W. F. Chen, Y. K. Lu, K. H. Chen, G. L. Lin, and S. C. Li, "Research on the disaster characteristics of three Ms>6 earthquakes in yunnan in 2014," *Journal of Seismological Research*, vol. 40, no. 1, pp. 144–152, 2017, (In Chinese).

[6] Y. Huang, L. Y. Zhao, M. Xiong, C. Liu, and P. Lu, "Critical slip surface and landslide volume of a soil slope under random earthquake ground motions," *Environmental Earth Sciences*, vol. 77, no. 23, p. 787, 2018.

[7] A. Kafaei Mohammadnejad, S. M. Mousavi, M. Torabi, M. Mousavi, and A. H. Alavi, "Robust attenuation relations for peak time-domain parameters of strong ground motions," *Environmental Earth Sciences*, vol. 67, no. 1, pp. 53–70, 2012.

[8] S. Lagomarsino and S. Cattari, "PERPETUATE guidelines for seismic performance-based assessment of cultural heritage masonry structures," *Bulletin of Earthquake Engineering*, vol. 13, no. 1, pp. 13–47, 2015.

[9] E. A. Dizaj, R. Madandoust, and M. M. Kashani, "Probabilistic seismic vulnerability analysis of corroded reinforced concrete frames including spatial variability of pitting corrosion," *Soil Dynamics and Earthquake Engineering*, vol. 114, pp. 97–112, 2018.

[10] Y. X. Hu, *Earthquake Engineering*, Seismological Press, Beijing, China, 2006.

[11] T. C. Hanks and H. Kanamori, "A moment magnitude scale," *Journal of Geophysical Research*, vol. 84, no. B5, p. 2348, 1979.

[12] Y. Shoji, K. Tanii, and M. Kamiyama, "A study on the duration and amplitude characteristics of earthquake ground motions," *Soil Dynamics and Earthquake Engineering*, vol. 25, no. 7-10, pp. 505–512, 2005.

[13] A. K. Chopra, "Earthquake resistant design of concrete gravity dams," *Journal of the Structural Division*, vol. 104, no. 6, pp. 953–971, 1978.

[14] Q. J. Chen, W. Z. Yuan, Y. C. Li, and L. Y. Cao, "Dynamic response characteristics of super high-rise buildings subjected to long-period ground motions," *Journal of Central South University*, vol. 20, no. 5, pp. 1341–1353, 2013.

[15] M. G. Tian and W. J. Yi, "Dynamic behavior of reinforced concrete frame structure during construction," *Journal of Central South University of Technology*, vol. 15, no. 3, pp. 418–422, 2008.

[16] N. E. Huang, Z. Shen, S. R. Long et al., "The empirical mode decomposition and the Hilbert spectrum for nonlinear and non-stationary time series analysis," *Proceedings of the Royal Society of London. Series A: Mathematical, Physical and Engineering Sciences*, vol. 454, no. 1971, pp. 903–995, 1998.

[17] J. C. Chen, L. M. Wang, P. Wang, and A. L. Che, "Failure mechanism investigation on loess-mudstone landslides based on the Hilbert-Huang transform method using a large-scale

shaking table test," *Engineering Geology*, vol. 302, p. 106630, Article ID 106630, 2022.

[18] S. R. Garcia, M. P. Romo, and L. Alcántara, "Analysis of nonlinear and non-stationary seismic recordings of Mexico City," *Soil Dynamics and Earthquake Engineering*, vol. 127, p. 105859, Article ID 105859, 2019.

[19] S. Chowdhury, A. Deb, M. Nurujjaman, and C. Barman, "Identification of pre-seismic anomalies of soil radon-222 signal using Hilbert-Huang transform," *Natural Hazards*, vol. 87, no. 3, pp. 1587–1606, 2017.

[20] Y. Changwei, F. Ning, Z. Jianjing, B. Junwei, and Z. Jun, "Research on time-frequency analysis method of seismic stability of covering-layer type slope subjected to complex wave," *Environmental Earth Sciences*, vol. 74, no. 6, pp. 5295–5306, 2015.

[21] T. Liu, Z. J. Luo, J. H. Huang, and S. Yan, "A comparative study of four kinds of adaptive decomposition algorithms and their applications," *Sensors*, vol. 18, no. 7, p. 2120, 2018.

[22] K. Dragomiretskiy and D. Zosso, "Variational mode decomposition," *IEEE Transactions on Signal Processing*, vol. 62, no. 3, pp. 531–544, 2014.

[23] M. Thomas, D. Zarour, S. Meziani, and M. Kedadouche, "Faulty bearing features by variational mode decomposition," *Vibroengineering PROCEDIA*, vol. 16, pp. 29–34, 2017.

[24] Y. F. Guo, Z. S. Zhang, T. Gong, J. B. Cao, and W. Z. Yang, "Generalized variational mode decomposition for interlayer slipping detection of viscoelastic sandwich cylindrical structures," *Measurement Science and Technology*, vol. 29, no. 9, p. 095001, Article ID 095001, 2018.

[25] C. Y. Li, J. Y. Zhang, W. Wang, K. Sun, and X. J. Shan, "The seismogenic fault of the 2021 Yunnan Yangbi M_S 6.4 earthquake," *Seismology and Geology*, vol. 43, no. 3, pp. 706–721, 2021, (In Chinese).

[26] Z. R. Pan, T. L. Li, J. W. Cui et al., "Characteristics of strong motion records of the Yangbi Ms 6.4 and related earthquakes on May 21, 2021," *China Earthquake Engineering Journal*, vol. 43, no. 4, pp. 791–798, 2021, (In Chinese).

[27] S. C. Liu, Y. K. Lu, Y. Zhou et al., "Characteristics of earthquake damage caused by the 2021 Yangbi, yunnan MS6. 4 earthquake," *Journal of Seismological Research*, vol. 44, no. 03, pp. 452–460, 2021, (In Chinese).

[28] H. C. Jia, F. Chen, Y. D. Fan, and D. H. Pan, "Comparison of two large earthquakes in China: the ms 6.6 yunnan Jinggu earthquake and the ms 6.5 yunnan ludian earthquake in 2014," *International Journal of Disaster Risk Reduction*, vol. 16, pp. 99–107, 2016.

[29] X. Chaoxu, N. Gaozhong, F. Xiwei, L. Huayue, Z. Junxue, and Z. Xun, "A new model for the quantitative assessment of earthquake casualties based on the correction of anti-lethal level," *Natural Hazards*, vol. 110, no. 2, pp. 1199–1226, 2022.

[30] B. Zhang, X. J. Li, M. S. Rong, Y. X. Yu, Y. S. Wang, and J. X. Wang, "Analysis of strong ground motion characteristics and earthquake damage for the Yangbi Ms 6.4 earthquake, Yunnan," *Seismology and Geology*, vol. 43, no. 5, pp. 1127–1139, 2021, (In Chinese).

[31] S. L. Kramer and M. W. Smith, "Modified Newmark model for seismic displacements of compliant slopes," *Journal of Geotechnical and Geoenvironmental Engineering*, vol. 123, no. 7, pp. 635–644, 1997.

[32] L. Agostini, J. Boaga, A. Galgaro, and A. Ninfo, "HVSR technique in near-surface thermal-basin characterization: the example of the Caldiero district (North-East Italy)," *Environmental Earth Sciences*, vol. 74, no. 2, pp. 1199–1210, 2015.

[33] J. D. Thornley, U. Dutta, J. Douglas, and Z. J. Yang, "Evaluation of horizontal to vertical spectral ratio and standard spectral ratio methods for mapping shear wave velocity across anchorage, Alaska," *Soil Dynamics and Earthquake Engineering*, vol. 150, Article ID 106918, 106918 pages, 2021.

[34] İT. Güven, "Seismic vulnerability indices for ground in Derince-Kocaeli (NW Turkey)," *Environmental Earth Sciences*, vol. 81, no. 5, p. 167, 2022.

[35] S. Yang, G. P. Mavroeidis, J. C. de la Llera et al., "Empirical site classification of seismological stations in Chile using horizontal-to-vertical spectral ratios determined from recordings of large subduction-zone earthquakes," *Soil Dynamics and Earthquake Engineering*, vol. 125, Article ID 105678, 105678 pages, 2019.

[36] Y. A. Nakamura, "Method for dynamic characteristics estimation of subsurface using microtremor on the ground surface," *Quarterly Report of Railway Technical Research Institute*, vol. 30, no. 1, pp. 25–33, 1989.

[37] P. B. Xu, R. Z. Wen, H. W. Wang, K. Ji, and Y. F. Ren, "Characteristics of strong motions and damage implications of M S6.5 Ludian earthquake on August 3, 2014," *Earthquake Science*, vol. 28, no. 1, pp. 17–24, 2015.

[38] P. B. Xu, R. Z. Wen, and Y. F. Wen, "Comparison of strong-motion records and damage implications between the 2014 Yunnan Ms 6.5 Ludian earthquake and Ms 6.6 Jinggu earthquake," *Earthquake Science*, vol. 31, no. 1, pp. 12–18, 2018.

[39] Z. Qu and X. Shi, "Comparative study on the pulse-like seismic signals in the Wenchuan and the Ludian earthquakes," *Engineering Mechanics*, vol. 33, no. 8, pp. 150–157, 2016, (In Chinese).

[40] R. Sehhati, A. Rodriguez-Marek, M. Eigawady, and W. F. Cofer, "Effects of near-fault seismic signals and equivalent pulses on multistory structures," *Engineering Structures*, vol. 33, no. 3, pp. 767–779, 2011.

[41] C. H. Zhai, S. Li, L. L. Xie, and Y. M. Sun, "Study on inelastic displacement ratio spectra for near-fault pulse-type ground motions," *Earthquake Engineering and Engineering Vibration*, vol. 6, no. 4, pp. 351–355, 2007.

[42] G. W. Housner and D. E. Hudson, "The port hueneme earthquake of march 18, 1957," *Bulletin of the Seismological Society of America*, vol. 48, no. 2, pp. 163–168, 1958.

[43] G. P. Mavroeidis and A. S. Papageorgiou, "A mathematical representation of near-fault ground motions," *Bulletin of the Seismological Society of America*, vol. 93, no. 3, pp. 1099–1131, 2003.

[44] J. W. Baker, "Quantitative classification of near-fault ground motions using wavelet analysis," *Bulletin of the Seismological Society of America*, vol. 97, no. 5, pp. 1486–1501, 2007.

[45] S. Mukhopadhyay and V. K. Gupta, "Directivity pulses in near-fault ground motions—I: identification, extraction and modeling," *Soil Dynamics and Earthquake Engineering*, vol. 50, pp. 1–15, 2013.